Hindawi
International Journal of Chemical Engineering
Volume 2022, Article ID 7413554, 12 pages
https://doi.org/10.1155/2022/7413554

Research Article

Design of an Adaptive Control to Feed Hydrogen-Enriched Ethanol-Gasoline Blend to an Internal Combustion Engine

J. García-Morales,[1] R. F. Escobar-Jiménez,[1] O. J. Ramos-Negrón,[2] D. A. Carbot-Rojas,[3] M. Cervantes-Bobadilla,[4] and J. F. Gómez-Aguilar[5]

[1]*Tecnológico Nacional de México, Centro Nacional de Investigación y Desarrollo Tecnológico, Int. Internado Palmira S/N, Palmira C.P.62490, Cuernavaca, Morelos, Mexico*
[2]*Tecnológico Nacional de México, ITS de las Choapas, Carretera Las Choapas-Cerro de Nanchital Km. 6.0 Col J. Mario Rosado C.P. 96980 Las Choapas, Veracruz, Mexico*
[3]*Centro Nacional de Metrología, Km. 4.5 Carretera a Los Cués S/N, C.P.76246, El Marqués, Querétaro, Mexico*
[4]*Universidad Autónoma del Estado de Morelos, Centro de Investigación en Ingeniería y Ciencias Aplicadas, Av. Universidad No. 1001 Col Chamilpa, C.P. 62209, Cuernavaca, Morelos, Mexico*
[5]*Conacyt-Tecnológico Nacional de México, Centro Nacional de Investigación y Desarrollo Tecnológico, Int. Internado Palmira S/N, Palmira C.P.62490, Cuernavaca, Morelos, Mexico*

Correspondence should be addressed to R. F. Escobar-Jiménez; esjiri@cenidet.edu.mx

Received 11 March 2022; Revised 30 September 2022; Accepted 22 October 2022; Published 7 November 2022

Academic Editor: Andreas Bück

In this work, an internal combustion (IC) engine air-fuel ratio (AFR) control system is presented and evaluated by simulation. The control scheme aims to regulate the overall air-fuel ratio (AFRoverall) in an IC engine fueled with a hydrogen-enriched ethanol-gasoline blend (E10) as fast as possible. The control scheme designed and developed in this work considers two control laws, a feedback control law to regulate the hydrogen and adaptive nonlinear control law for controlling the E10 mass flow injection. The main contribution of this work is the reduction of the number of controllers used for controlling the overall air-fuel ratio since other control strategies use two controllers for controlling the E10 mass flow injection. Simulation results have shown the effectiveness of the new control scheme.

1. Introduction

Due to IC engines' ability to be fueled with alternative fuels, such as ethanol, keeping the IC engine's air-fuel ratio at the optimum stoichiometric value becomes a complex problem to solve. In the automatic control area in the last decades, different control strategies have been developed and implemented by various authors to deal with this problem, e.g., observer-based control, intelligent control [1], and model-based control [2, 3].

Concerning the design of observer-based controllers, in [4], two types of nonlinear observers were developed and tested to solve the problem of the mass airflow estimation. A constant gain extended Kalman filter (CGEKF) and sliding mode observer (SMO) were the two observers used in this work. The experimental results have shown that the extended Kalman filter performance was superior to the SMO. The authors in [5] developed an observer-based control for the IC engine AFR control. The results showed the effectiveness of the proposed strategy. The authors concluded that designing the AFR control by using state observers aids in providing improved control. On the other hand, in [6], a nonlinear observer-based control scheme incorporating the hybrid extended Kalman filter (HEKF) and a dynamic sliding mode control (DSMC) was designed and simulated. The simulation results showed a superior regulation of the air-fuel ratio control using the sliding mode plus the extended Kalman filter. The authors

in [7] proposed an active disturbance rejection control (ADRC) with an adaptive extended state observer (AESO) to deal with the uncertainties of the plant and the sensors. Experimental results have shown that the proposed controller ensures accuracy despite the plant uncertainties and the measurement noise.

Intelligent control is another technique used for controlling the AFR. In [8], an air-fuel ratio control based on artificial intelligence was designed and simulated to reduce exhaust emissions. The simulation results showed that the AFR allows keeping within 0.5% of the set stoichiometric value. Based on a Takagi–Sugeno model, authors in [9] designed an AFR nonlinear control law for an IC engine fueled with gasoline. The simulation results showed the effectiveness of the control law. The authors in [10] developed an online sequential extreme learning machine (OEMPC), comparing its performance with the diagonal recurrent neural network MPC and a conventional PID controller. The authors mentioned that experimental results showed superior performance of the OEMPC over the other two controllers.

The model-based control technique, as the other two control techniques previously mentioned, has been another option for researchers to design controllers. Authors in [11] developed an adaptive AFR control scheme. The authors presented a static AFR calculation model based on in-cylinder pressure data and the adaptive AFR control strategy. The experimental results showed the effectiveness of the control technique. Authors in [12] implemented an internal model controller (IMC) combined with a discrete adaptive controller for controlling the AFR with parametric uncertainties. The simulation results showed the effectiveness of the proposed method. In [13], two adaptive controllers for the AFR control were developed and experimentally tested. The first adaptive controller was based on a feedforward control adaptation, while the second design consisted of feedback control and feedforward adaptation incorporating the adaptive posicast controller (APC). Experimental results showed the effectiveness of the APC to solve the AFR problem. Authors in [14] developed a model-reference adaptive control for controlling the AFR. Since the system dynamics exhibit nonlinearities, the authors used an extended Kalman filter for parameter identification. The experimental results showed the effectiveness of the method.

Regarding the AFR control of IC engine fueled with multiple fuels (gasoline-ethanol-hydrogen), authors in [15] presented a control scheme for an IC engine feed with a hydrogen-enriched E10 blend, and the aim of the control scheme was for controlling the AFR. The authors showed the effectiveness of the control scheme based on PI controllers by simulation results. Afterwards, the authors in [16] validate the same control scheme experimentally.

Recently, the authors in [17] proposed a unified fault-tolerant control system (UFTCS) based on advanced analytical and hardware redundancies for air-fuel ratio (AFR) control of spark ignition (SI) internal combustion (IC) engines. The authors proposed a new methodology based on active and passive fault-tolerant control. The authors carried out a comparison with the existing AFR control systems to show the performances of the controllers. The authors in [18] presented a novel passive fault tolerant control system (PFTCS) for the air-fuel ratio (AFR) control system of an IC gasoline engine to prevent its shutdown. The authors in [19] developed an AFR control strategy in lean-burn spark-ignition engines by proposing a genetic algorithm (GA)-based proportional-integral (PI) control technique. The results demonstrated the accurate regulation of the AFR under various operating conditions of the IC engines. The authors in [20] have shown the advantages of employing the sliding mode controller for AFR control over comparisons to the proportional-integral-derivative (PID) controller. Finally, in [21], a composite predictive control method based on a wavelet network was proposed to achieve accurate control of the transient air-fuel ratio for gasoline engines. The control strategy had high performances and could improve the control precision of the AFR during transience.

In this work, an adaptive controller is developed for controlling the stoichiometric ratio in an IC engine fueled with an ethanol-gasoline hydrogen-enriched blend due to the importance of keeping the AFR regulated despite disturbances. The controller's goal is to control the AFR of an IC engine fed with multiple fuels considering constant disturbances. The design of an adaptive nonlinear control law was performed by the Lyapunov analysis ensuring the system stability. The purpose of the adaptive nonlinear controller is to replace the feedforward and feedback controller developed in [16] to regulate the IC engine AFR taking into account the cylinder port fuel flow, speed, and pressure disturbances.

This manuscript is organized as follows: Section 2 described the internal combustion engine model. Experimental polynomials are shown to calculate the discharge coefficient, the volumetric efficiency, and the combustion efficiency. Section 3 presents the adaptive control strategy. Sections 4 and 5 show the results and conclusions of this work.

2. Internal Combustion Engine

Figure 1 shows the IC engine benchmark, and model parametrization was carried out by using the IC engine's experimental data. The IC engine is 1.6 l, 78 kW. Table 1 shows the parameters of the IC engine, and Table 2 shows the nomenclature used to develop this work.

2.1. Internal Combustion Engine Model. Five submodels of the IC engine were used to develop the control law: fuel dynamic, airflow dynamic, air mass into the cylinder, air-fuel ratio, and work exercised by the gas.

2.2. Fuel Injection System. For calculating the entering fuel flow into the combustion chamber, it is necessary to calculate the fuel film flow injected into the cylinder as a liquid ($\dot{m}_{fl}$) and vapor ($\dot{m}_{fv}$) [22].

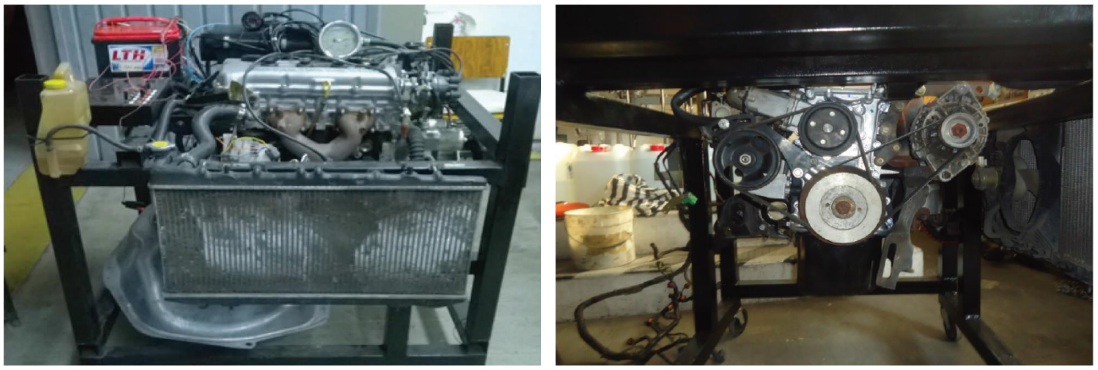

Figure 1: IC engine and electrolyzer.

Table 1: IC engine parameters.

Number of cylinders	4
Cylinder displacement volumetric	1.595 m^3
Maximum power	78 kW/6000 rpm
Maximum torque	138 Nm/4000 rpm
Compression ratio	9.5:1
Ratio of cylinder bore to piston stroke	0.863
Valves	4 valves/cylinder
Minimum regime	625 rpm
Maximum regime	6000 rpm
Throttle radio	50 mm
Manifold volume	0.00148 m^3
Stoichiometric air-fuel ratio (gasoline)	14.6

$$\dot{m}_{fl} = X\dot{m}_{fi} - \frac{1}{\tau_{fl}} m_{fl},$$
$$\dot{m}_{fv} = (1 - X)\dot{m}_{fi}, \quad (1)$$
$$\dot{m}_f = \dot{m}_{fv} + \frac{1}{\tau_{fl}} m_{fl},$$

where X denotes a fraction, $\dot{m}f_i$ is the injected fuel mass flow, $\dot{m}_f$ is the fuel flow feed into the cylinders, and $1/\tau_{f_l}$ is the fuel film evaporation time constant (s) [22].

Table 2: Nomenclature.

Symbols	A	Throttle flow area, m^2
	$H_{2(g)}$	Hydrogen gas
	$H_2O_{(l)}$	Liquid water
	J	Current, A
	j	Current density, Am^2
	m_f	Cylinder port fuel flow, $\%kg/s$
	m_r	Residual mass, kg
	nc	Number of cells in series per stack
	O_2	Oxygen gas
	T_a	Atmosphere temperature, K
Constants	F	Faraday constant, 96487 $Cmol^{-1}$
	k	Ratio of specific heats, $k = 1.4$
	P_a	Atmosphere pressure, $101.315kPa$
	R	Constant air, $0.287kJ/kgK$
	τ_{fl}	Fuel evaporation time constant $(0.25s)$
	z	2 number of electrons

2.3. Air Flow Dynamic. According to [23], the mass flow rate ($\dot{m}_{at}$) of air entering through the throttle valve is calculated as follows:

$$\dot{m}_{at}(\alpha, \phi) = \frac{AP_a}{\sqrt{RT_a}} \mathrm{CdF}(\alpha) F(\phi),$$
$$\phi = \frac{P_a}{P_m},$$
$$F(\phi) \begin{cases} P_m \geq P_c, & \left(\frac{P_m}{P_a}\right)^{1/k} \sqrt{\frac{2k}{k-1}\left[1 - \left(\frac{P_m}{P_a}\right)^{(k-1)/k}\right]} P_c = \left(\frac{2}{k+1}\right)^{k/(k-1)} P_a, \\ \text{otherwise}, & \frac{1}{\sqrt{2}}. \end{cases} \quad (2)$$

where A is the transversal area of the throttle valve, R is the air constant, P_a, P_c, are the atmosphere and critical pressures, respectively, and Pm is the pressure in the manifold. The specific heat ratio is represented by $k = cp/cv$, T_a is the atmosphere temperature, Cd is the discharge coefficient, and $F(\alpha)$ and $F(\varphi)$ are the section factor and the pressure factor, respectively.

A polynomial function based on experimental data to calculate Cd and $F(\alpha)$ is proposed in

$$\mathrm{CdF}(\alpha) = -6.659 \times 10^{-14}\alpha^5 + 1.197 \times 10^{-2}\alpha^4 - 43.219\alpha^3 + 5.794\alpha^2 - 34.102\alpha + 74.395. \tag{3}$$

Equation (4) is applied to calculate the mass flow rate ($\dot{m}_{acyl}$) of air entering into the cylinders [24].

$$\dot{m}_{acyl} = \frac{30V}{3600\,RT_m} nP_m\eta_{vol}, \tag{4}$$

where V is the cylinder displacement volume, n is engine speed, and η_{vol} is the cylinder volumetric efficiency.

The volumetric efficiency (η_{vol}) for an engine without load is calculated by the polynomial function.

$$\eta_{\mathrm{vol}}(n) = a_5n^5 + a_4n^4 + a_3n^3 + a_2n^2 + a_1n + a_0, \tag{5}$$

where $a_5 = 1.378 \times 10^{-17}$, $a_4 = -1.039 \times 10^{-13}$, $a_3 = 3.096 \times 10^{-10}$, $a_2 = -4.718 \times 10^{-07}$, and $a_1 = 3.515 \times 10^{-04}$, $a_0 = 3.526 \times 10^{-01}$

2.4. Intake Manifold Temperature and Pressure. The intake manifold temperature (T_m) and pressure (P_m) are calculated by equations (6) and (7), respectively [25].

$$\frac{\mathrm{d}T_m}{\mathrm{d}t} = \frac{R}{V_m}\frac{T_m}{P_m}\left[\dot{m}_{at}(kT_a - T_m) - \dot{m}_{\mathrm{acyl}}(k-1)T_a\right], \tag{6}$$

$$\frac{dP_m}{dt} = \frac{RT_m}{V_m}\left(\dot{m}_{at} - \dot{m}_{acyl}\right), \tag{7}$$

where V_m is the volume in the intake manifold, $\dot{m}_{at}$ is the mass flow rate of air entering through the throttle valve, and $\dot{m}_{acyl}$ is the mass flow rate of air entering into the cylinders.

2.5. Air and Hydrogen Volume and Mass Calculations. For estimating the hydrogen feed to the IC engine, it is necessary to consider the effect of ethanol and hydrogen percentage in the fuel blend, and thus, the following assumptions are considered:

(i) The air and hydrogen volume cannot overpass the cylinder displacement volume.

(ii) The AFR ratio should be considered.

To estimate the volumes, the ideal gases' equation is considered.

$$m_{air} = \frac{P_mV_{air}}{R_{air}T_m}, \tag{8}$$

where m_{air}, V_{air}, and R_{air} are the air mass, the air volume, and the air constant, respectively.

$$m_H = \frac{P_mV_H}{R_HT_m}, \tag{9}$$

where m_H, V_H, and R_H are the hydrogen mass, the hydrogen volume, and the hydrogen constant, respectively.

$$\frac{m_{air}}{m_H} = AFR_H, \qquad \frac{V_{air}R_H}{V_HR_{air}} = AFR_H. \tag{10}$$

The air and hydrogen volumes are calculated as follows:

$$V_{air} = \frac{AFR_HR_{air}}{R_H}V_H, \tag{11}$$

$$V_H = \frac{R_HV_{air}}{AFR_HR_{air}}. \tag{12}$$

From the inequality $V_{\mathrm{air}} + V_H \le \eta_{\mathrm{vol}}V$, it is possible to estimate the maximum amount of hydrogen to be fed into the IC engine, maintaining an adequate AFR without exceeding the product between $\eta_{vol}V$.

Then, the inequality previously mentioned is formulated to calculate $V_{air} = \eta_{\mathrm{vol}}V - V_H$ and $V_H = \eta_{\mathrm{vol}}V - V_{\mathrm{air}}$, and by substituting, V_{air} and V_H from Equations (11) and (12), respectively, equations (13) and (14) are obtained.

$$V_{\mathrm{air}} = \frac{\eta_{\mathrm{vol}}V(AFR_H)R_{\mathrm{air}}}{(AFR_H)R_{\mathrm{air}} + R_H}, \tag{13}$$

$$V_H = \frac{\eta_{\mathrm{vol}}\mathrm{VR}_H}{(AFR_H)R_{\mathrm{air}} + R_H}. \tag{14}$$

From Equations (13) and (14), and from the ideal gas equation, the hydrogen and the air mass are calculated as follows:

$$m_{air} = \frac{\eta_{\mathrm{vol}}P_mV(AFR_H)}{T_m(AFR_HR_{\mathrm{air}}) + R_H}, \qquad m_H = \frac{\eta_{\mathrm{vol}}P_mV}{T_m(AFR_H)R_{\mathrm{air}} + R_H}. \tag{15}$$

2.6. Thermal Efficiency. Considering the optimum ignition angle, the thermal efficiency of the engine η_t was calculated as follows [26]:

$$\begin{aligned}\eta_t &= \eta_{to}\eta_t(P_m)\eta_t(\lambda, n)\eta_t(n),\\ \eta_t(P_m) &= \eta_{tp0} + \eta_{tp1}P_m + \eta_{tp2}P_m^2,\\ \eta_t(\lambda, n) &= \eta_{t\lambda 0} + \eta_{t\lambda 1}\lambda + \eta_{t\lambda 2}\lambda^2 + \eta_{t\lambda 3}n,\\ \eta_t(n) &= \eta_{tn0} + \eta_{tn1}e^{n/\eta_{tn2}},\end{aligned} \tag{16}$$

where $\eta_{t0} = 0.4593$, $\eta_{tp0} = 0.474$, $\eta_{tp1} = 0.01664$, $\eta_{tp2} = -0.0001315$, $\eta_{t\lambda 0} = -1.34$, $\eta_{t\lambda 1} = 5.3906$, $\eta_{t\lambda 2} = -3.1043$, $\eta_{t\lambda 3} = 1.43 \times 10^{-6}$, $\eta_{tn0} = -0.8243$, $\eta_{tn1} = 1.577$, and $\eta_{tn2} = 42740$

2.7. Combustion Efficiency. In [27,28], the authors reported that using a gasoline-ethanol blend as fuel, the combustion efficiency of the IC engine can be improved because of the oxygen present in the ethanol molecular structure. Equation (17) was proposed in [29] to calculate the combustion efficiency of the gasoline-ethanol blend.

$$\eta_c = C_{\text{burn}}\eta_{ac}(\lambda)\eta_{\eta v}(\eta_v). \tag{17}$$

In this work, to calculate the combustion efficiency of the IC engine, the polynomial Equation (18) is proposed, which considers the hydrogen influence [16].

$$\begin{aligned}\eta_{H2} &= 3.040 \times 10^{-5}Hm^5 - 4.393 \times 10^{-4}Hm^4\\ &+ 1.846 \times 10^{-3}Hm^3 - 6.801 \times 10^{-4}Hm^2\\ &+ 1.859 \times 10^{-5}Hm + 1.\end{aligned} \tag{18}$$

Then, combustion efficiency is calculated as follows :

$$\eta_c = C_{\text{burn}} \cdot \eta_{ac}(\lambda) \cdot \eta_{\eta v}(\eta_v) \cdot \eta_{H2}. \tag{19}$$

2.8. Air-Fuel Ratio. According to [15], Equation (20) is used to calculate the air-fuel ratio of the hydrogen-enriched E10 blend.

$$\text{AFR} = 9Em + 14.6[1 - (Em + Hm)] + 34.33Hm, \tag{20}$$

where Hm is the known hydrogen fraction added to the blend and Em is the ethanol fraction contained in the ethanol-gasoline blend.

Equation (21) is applied to verify that the combustion performs adequately, determining if the AFR is lean or rich.

$$\lambda = \frac{m_{acyl}}{14.6m_g + 9m_E + 34.3m_H}, \tag{21}$$

where m_g, m_E, and m_H are the mass of gasoline, the mass of ethanol, and the mass of hydrogen, respectively.

3. Control Strategy

In previous work [16], a control scheme based on two feedback PIs controllers and a feedforward control was presented to control the overall AFR of an IC engine. The first feedback PI controller was used to control hydrogen production, while the feedback and feedforward controllers were used to estimate the E10 blend flow rate and the injection time based on the mass flow rate of the air, respectively. To reduce the number of controllers used for controlling the AFR of an IC engine fueled with a hydrogen-enriched E10 blend and considering constant disturbances, this work presents the design of an adaptive nonlinear control law. The purpose of the nonlinear controller is to replace the feedforward and feedback controller developed in [16] to regulate the internal combustion engine AFR considering the disturbances caused by the use of a fuel blend.

The first step to design the control law is to define the state variables as follows: $(x_1, x_2, x_3) = (\dot{m}_f, n, P_m)$, where $\dot{m}_f$ is the cylinder port fuel flow, n is the engine speed, and P_m is the pressure in the manifold. Then, the fuel flow dynamic is defined by

$$\begin{aligned}\dot{x}_1 &= \frac{d\dot{m}_f}{dt} = \frac{1}{\tau_{fl}}\left(-\dot{m}_f + \dot{m}_{fi}\right) + (1 - X)\frac{d\dot{m}_{fi}}{dt},\\ \dot{x}_1 &= \frac{1}{\tau_{fl}}(-x_1 + u) + (1 - X)\frac{d\dot{m}_{fi}}{dt}.\end{aligned} \tag{22}$$

Now, to let the crankshaft speed be a state variable, we consider the following equations to determine the engine acceleration:

$$W_{\text{net}} = m_t\eta_t\eta_c\frac{Q_{\text{LHV}}}{\text{AFR}_e + 1}\left(1 - \frac{m_r}{m_t}\right), \tag{23}$$

where the total mass in the cylinder is defined as m_t,

$$m_t = m_f + m_{acyl}. \tag{24}$$

So, to calculate the total mass per cycle, we started calculating the mass flow rate in the cylinder and the volumetric efficiency in function of the engine speed.

$$\dot{m}_{\text{acyl}} = \left(\frac{30V}{3600\text{RT}_m}P_m n\right)\eta_{vol}, \tag{25}$$

$$\eta_{\text{vol}}(n) = a_5n^5 + a_4n^4 + a_3n^3 + a_2n^2 + a_1n + a_0. \tag{26}$$

Substituting the state variables into equation (25) and renaming the variables, we have the following equation:

$$\dot{m}_{acyl} = z\left(a_5x_2^5 + a_4x_2^4 + a_3x_2^3 + a_2x_2^2 + a_1x_2 + a_0\right), \tag{27}$$

where $z = (30V/3600\text{RT}_m)x_3x_2$ and a_i are the polynomial coefficients

Now, to get the total mass per cycle we have the following equation:

$$m_t = \frac{x_1 + z\left(a_5x_2^5 + a_4x_2^4 + a_3x_2^3 + a_2x_2^2 + a_1x_2 + a_0\right)}{(n/120)}. \tag{28}$$

The losses due to friction torque and pumping are represented by L_{tp} in the following equation:

$$L_{tp} = 2.029 \times 10^{-21} x_2^7 - 2.871 \times 10^{-17} x_2^6 + 1.706 \times 10^{-13} x_2^5 - 5.514 \times 10^{-10} x_2^4 + 1.045 \times 10^6 x_2^3 - 1.162 \times 10^{-3} x_2^2 + 6.982 \times 10^{-1} x_2 - 1.535 \times 10^2. \tag{29}$$

So, we can represent the crankshaft acceleration by

$$\cdot x_2 = \frac{\mathrm{d}n}{\mathrm{d}t} = \frac{\left[\left(m_t \eta_t \eta_c \eta_m \left(Q_{LHV}/AFR_e + 1\right)\left(1 - \left(m_r/m_t\right)\right)(0.25/\pi)\right) - L_{tp}\left(x_2\right)\right]}{I}. \tag{30}$$

The intake manifold pressure is represented by the following equation considering that $\mathrm{CdF}(\alpha) = f(\alpha)$.

$$\cdot x_3 = \frac{dP_m}{dt} = \left[\begin{pmatrix} \phi^{1/k}\sqrt{(2k/k-1)\left(1-\phi^{(k-1/k)}\right)}, x_3 \geqq P_c \\ \dfrac{RT_m P_a A}{V_m\sqrt{RT_a}} \\ \sqrt{k\left(\dfrac{2}{k+1}\right)^{(k+1)/(k-1)}}, x_3 < P_c \end{pmatrix} f(\alpha) - \left[\frac{\dot{m}_{acyl}}{3600}\right]\right], \tag{31}$$

$$\mathrm{CdF}(\alpha) = f(\alpha) = -6.66 \times 10^{-14}\alpha^5 + 1.19 \times 10^{-2}\alpha^4 - 4.32 \times 10^{-01}\alpha^3 + +5.79\alpha^2 - 34.1\alpha + 74.4.$$

The nonlinear model is described in the general form by equation (32).

$$\begin{aligned} \dot{x}(t) &= f(x(t)) + G\tilde{u}(t), \\ y(t) &= \hat{h}(x(t)). \end{aligned} \tag{32}$$

To design the control law, the model consists of three state variables $(x_1, x_2, x_3) = (\dot{m}_f, n, P_m)$, variables, one manipulated variable $(u = \dot{m}_{fi})$, and one output $(y = \lambda)$, assuming that $T_m = T_a$.Defining the nonlinear system presented in (32),

$$\dot{x} = \underbrace{\begin{bmatrix} \dfrac{-x_1}{\tau_{fl}} \\ \dfrac{\left[\left(m_t \eta_t \eta_c \eta_m \left(Q_{LHV}/\left(AFR_e + 1\right)\right)\left(1 - \left(m_r/m_t\right)\right)(0.25/\pi)\right) - L_{tp}\left(x_2\right)\right]}{I} \\ \begin{pmatrix} \varphi^{1/k}\sqrt{\dfrac{2k}{k-1}\left(1-\varphi^{k-1/k}\right)}, x_3 \geqq P_c \\ \dfrac{RT_m P_a A}{V_m\sqrt{RT_a}} \\ \sqrt{k\left(\dfrac{2}{k+1}\right)^{\dfrac{k+1}{k-1}}}, x_3 < P_c \end{pmatrix} f(\alpha) - \left[\dot{m}_{acyl}/3600\right] \end{bmatrix}}_{f(x)} + \underbrace{\begin{bmatrix} 1 & 0 & 0 \\ 0 & 1 & 0 \\ 0 & 0 & 1 \end{bmatrix}}_{G} \underbrace{\begin{bmatrix} \dfrac{u}{\tau_{fl}} + (1-X)\dfrac{d\dot{m}_{fi}}{dt} \\ 0 \\ 0 \end{bmatrix}}_{} \tilde{u}, \tag{33}$$

where $\tilde{u} = [\tilde{u}_1, 0, 0]^T$, so the term that depends of the control input to be designed is $\tilde{u}_1$. Since $= h(x)$, then $h(x) = \lambda$ is the controlled variable, which is expressed as follows:

$$\hat{h}(x) = \begin{bmatrix} \lambda \\ x_2 \\ x_3 \end{bmatrix}. \tag{34}$$

For designing the control law, a constant uncertainty for each state is assumed as follows:

$$\begin{bmatrix} \cdot x_1(t) \\ \cdot x_2(t) \\ \cdot x_3(t) \end{bmatrix} = \begin{bmatrix} f_1(x(t)) + g_1\tilde{u}_1 + d_1 \\ f_2(x(t)) + d_2 \\ f_3(x(t)) + d_3 \end{bmatrix}. \tag{35}$$

The system output is defined as $y_1 = \lambda$. So, the error can be defined as $e_1 = y_1 - r$, where r is the set point, so the dynamic error due to the state variable variations is defined as follows:

Considering that $\dot{e}_1 = \dot{y}_1 - \dot{r}$, then $\dot{e}_1 = \dot{y}_1$.

$$\begin{aligned} \cdot y_1 = \cdot e_1 &= \frac{\partial h}{\partial x}\dot{x} = \frac{\partial h}{\partial x_1}\cdot x_1 + \frac{\partial h}{\partial x_2}\cdot x_2 + \frac{\partial h}{\partial x_3}\cdot x_3 \\ &= \left(\frac{\partial h}{\partial x_1}f_1 + \frac{\partial h}{\partial x_2}f_2 + \frac{\partial h}{\partial x_3}f_3\right) + \left(\frac{\partial h}{\partial x_1}g_1\tilde{u}_1\right) + \left(\frac{\partial h}{\partial x_1}d_1 + \frac{\partial h}{\partial x_2}d_2 + \frac{\partial h}{\partial x_3}d_3\right). \end{aligned} \tag{36}$$

Equation (36) is rewritten as follows:

$$\cdot e_1 = L_h f + L_h g_1 \tilde{u}_1 + L_h \theta, \tag{37}$$

where $L_h = [L_{h_1} L_{h_2} L_{h_3}] = [\partial h/\partial x_1 \partial h/\partial x_2 \partial h/\partial x_3]$ and $f = [f_1 f_2 f_3]^T$, $\theta = [d_1 d_2 d_3]^T$.

Each one of the values of Lig_i depends on the state variables x. It could be supposed that $L_{hi}g_i$ and g_i are not zero for the range of the state variables. Thus, the inverse functions of $L_{h_j}g_i$ and g_i exist for this range.

$$\cdot e_1 = L_{h_1}g_1\left(\left(L_{h_1}g_1\right)^{-1}L_h f + \left(L_{h_1}g_1\right)^{-1}L_h\theta\right). \tag{38}$$

Considering that θ is the unknown parameter, as well as considering Barbalat's theorem, the close-loop error dynamics for an adaptive control law with an unknown parameter are calculated as follows [30]:

$$\dot{e} = -e + \Theta \cdot \psi, \tag{39}$$

where Θ is the parameter error and ψ is a bounded function of time t, in such a way that our system is represented as follows:

$$\cdot e_1 = -Ce_1 + (\theta - \hat{\theta})^T \cdot L_h^T, \tag{40}$$

where $C > 0$ represents a constant.

Once the close-loop error dynamics for an adaptive control law with an unknown parameter have been proposed, it is substituted in Equation (38) as follows:

$$-Ce_1 + (\theta - \hat{\theta})^T \cdot L_h^T = L_{h_1}g_1\left(\left(L_{h_1}g_1\right)^{-1}L_h f + \tilde{u}_1 + \left(L_{h_1}g_1\right)^{-1}L_h\theta\right). \tag{41}$$

Then, isolating $\tilde{u}_1$ in Equation (41), the control signal is represented by Equation (42) since there is only one control input $\tilde{u}_1$.

$$\tilde{u}_1 = -C\left(L_{h_1}g_1\right)^{-1}e_1 - \left(L_{h_1}g_1\right)^{-1}L_h f - \left(L_{h_1}g_1\right)^{-1}L_h\hat{\theta}, \tag{42}$$

With the purpose of estimating parameter θ, an adaptive law is obtained from the Lyapunov analysis as is presented in [31].

$$V = \frac{1}{2}e^2 + \frac{1}{2q}(\theta - \hat{\theta})^T(\theta - \hat{\theta}), \tag{43}$$

$$\dot{V} = e\dot{e} + \frac{1}{q}(\theta - \hat{\theta})^T(-\hat{\theta}), \tag{44}$$

$$\dot{V} = e_1\left(-Ce_1 + (\theta - \hat{\theta})^T \cdot L_h^T\right) + \frac{1}{q}(\theta - \hat{\theta})^T(-\hat{\theta}), \tag{45}$$

$$\dot{V} = -Ce_1^2 + e_1(\theta - \hat{\theta})^T \cdot L_h^T + \frac{1}{q}(\theta - \hat{\theta})^T(-\hat{\theta}), \tag{46}$$

$$\dot{V} = -Ce_1^2 + \frac{1}{q}(\theta - \hat{\theta})^T\left(q \cdot L_h^T e_1 - \hat{\theta}\right). \tag{47}$$

Based in Equation (47), with the aim to $\dot{V} \le 0$, the parametric update law is as follows:

$$\left(q \cdot L_h^T e_1 - \hat{\theta}\right)\hat{\theta} = qL_h^T e_1, \tag{48}$$

where the adaptation rate is $q > 0$. Substituting and carrying out the corresponding operations, we have

$$\begin{aligned}
\frac{\partial h}{\partial x_1} &= \left(\frac{30Vx_3x_2}{3600RT_m x_1^2}\right)\left(-a_5x_2^5 + a_4x_2^4 - a_3x_2^3 + a_2x_2^2 - a_1x_2 - a_0\right),\\
\frac{\partial h}{\partial x_2} &= \left(\frac{30Vx_3}{3600RT_m x_1}\right)\left(6a_5x_2^5 - 5a_4x_2^4 + 4a_3x_2^3 - 3a_2x_2^2 + 2a_1x_2 + a_0\right),\\
\frac{\partial h}{\partial x_3} &= \left(\frac{30Vx_2}{3600RT_m x_1}\right)\left(a_5x_2^5 - a_4x_2^4 + a_3x_2^3 - a_2x_2^2 + a_1x_2 + a_0\right),\\
L_h f &= \left[\left(\frac{30Vx_3x_2}{3600RT_m x_1^2}\right)\left(-a_5x_2^5 + a_4x_2^4 - a_3x_2^3 + a_2x_2^2 - a_1x_2 - a_0\right)\right]\frac{-x_1}{\tau_{fl}}\\
&\quad + \left(\frac{30Vx_3}{3600RT_m x_1}\right)\left(6a_5x_2^5 - 5a_4x_2^4 + 4a_3x_2^3 - 3a_2x_2^2 + 2a_1x_2 + a_0\right)\cdot x_2\\
&\quad + \left(\frac{30Vx_2}{3600RT_m x_1}\right)\left(a_5x_2^5 - a_4x_2^4 + a_3x_2^3 - a_2x_2^2 + a_1x_2 + a_0\right)\cdot x_3.
\end{aligned} \tag{49}$$

So, the control input $\tilde{u}_1$ can be expressed as follows:

$$\begin{aligned}
\tilde{u}_1 = &-C\left[\left(\frac{30Vx_3x_2}{3600RT_m x_1^2}\right)\left(-a_5x_2^5 + a_4x_2^4 - a_3x_2^3 + a_2x_2^2 - a_1x_2 - a_0\right)g_1\right]^{-1} e_1\\
&-\left[\left(\frac{30Vx_3x_2}{3600RT_m x_1^2}\right)\left(-a_5x_2^5 + a_4x_2^4 - a_3x_2^3 + a_2x_2^2 - a_1x_2 - a_0\right)g_1\right]^{-1}\cdot\\
&\left\{\begin{array}{l}
\left(\frac{30Vx_3x_2}{3600RT_m x_1^2}\right)\left(-a_5x_2^5 + a_4x_2^4 - a_3x_2^3 + a_2x_2^2 - a_1x_2 - a_0\right)\frac{-x_1}{\tau_{fl}}\\
+\left(\frac{30Vx_3}{3600RT_m x_1}\right)\left(6a_5x_2^5 - 5a_4x_2^4 + 4a_3x_2^3 - 3a_2x_2^2 + 2a_1x_2 + a_0\right)\cdot x_2\\
+\left(\frac{30Vx_2}{3600RT_m x_1}\right)\left(a_5x_2^5 - a_4x_2^4 + a_3x_2^3 - a_2x_2^2 + a_1x_2 + a_0\right)\cdot x_3
\end{array}\right\}\\
&-\left[\left(\frac{30Vx_3x_2}{3600RT_m x_1^2}\right)\left(-a_5x_2^5 + a_4x_2^4 - a_3x_2^3 + a_2x_2^2 - a_1x_2 - a_0\right)g_1\right]^{-1}\cdot L_h\hat{\theta}.
\end{aligned} \tag{50}$$

The proposed control law will allow reducing the errors caused by using two control signals as was formulated previously in the literature by [16] improving the dosage of the E10 blend to the IC engine and considering constant disturbances in the cylinder port fuel flow, speed, and pressure. To ensure the system stability, the control law was obtained from the Lyapunov analysis. The control scheme aims to ensure the correct fuel dosage (hydrogen-enriched E10 blend) into the IC engine since the hydrogen mass induced into the cylinders is 3.5%, corresponding to the 8% of the air-feed into the cylinders/cycle. Figure 2 shows the proposed control scheme for the overall AFR control.

4. Results

This section presents the simulation results of an adaptive controller used for controlling the E10 blend flow rate in an IC engine fueled with a hydrogen-enriched E10 blend. The controller aims to keep the AFR operating adequately. The

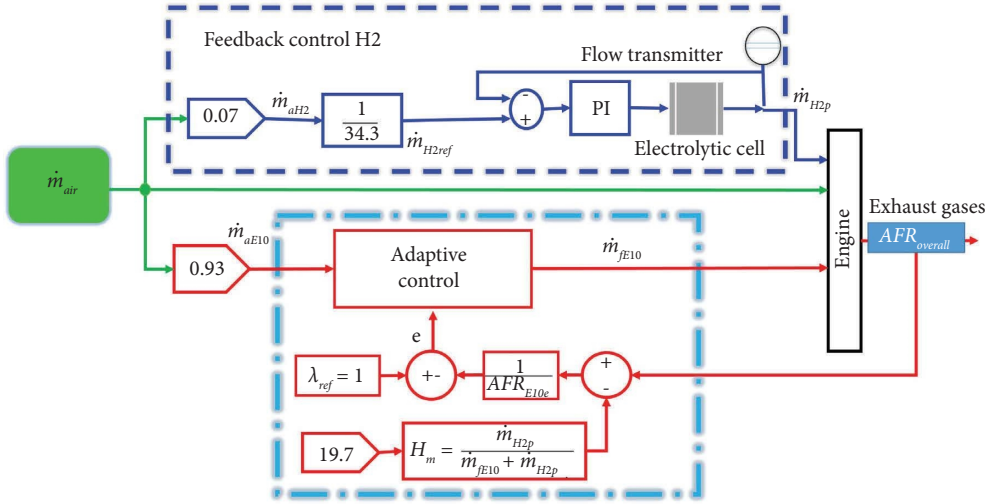

Figure 2: AFR control scheme.

simulations results are compared to those obtained with a PI controller presented in [15,16].

The crankshaft speed of the IC engine is shown in Figure 3. During this test, the crankshaft speed was varied between 1500 rpm and 2900 rpm to evaluate the performance of the adaptive controller.

The results of the AFR regarding the E10 blend are presented in Figure 4. The results showed that the adaptive controller adjusts the E10 blend injection into the cylinders rapidly to keep the AFR at the setpoint at each operating point. Moreover, the adaptive controller overshoots were lower in magnitude than those generated by the PI. It is due to the fast action of the adaptive controller.

The performance of the adaptive controller was evaluated and compared with a PI controller performance. Table 3 shows the performance evaluation of both controllers using the root mean square error (RMSE) and (mean square error) MSE errors.

For complementing the evaluation of the adaptive controller, an AFR error analysis is shown in Figure 5. The $AFRE10_{ref}$ setpoint is 14.04, and the system error is the difference between the controlled signal $AFRE10$ and the setpoint. The figure shows that the adaptive control action is faster than the PI control response. Moreover, it is shown how the AFR error obtained with the adaptive controller converges to zero before that obtained with the PI.

Figure 6 shows the overall $AFR_{overall}$ control for the hydrogen-enriched E10 blend using two different controllers (a PI controller and an adaptive controller) (the $AFR_{overall}$ represents the air-fuel ratio using a hydrogen-enriched E10 blend); also, Figure 6 shows that the adaptive control action is faster than the PI control action since the signal establishment time is lower for the adaptive control, and in addition, the adaptive controller overshoots were lower in magnitude in comparison to the PI controller overshoots. In consequence, the PI error will converge to zero more slowly than the adaptive control error.

The performance of the adaptive controller for controlling the overall $AFR_{overall}$ was evaluated and compared

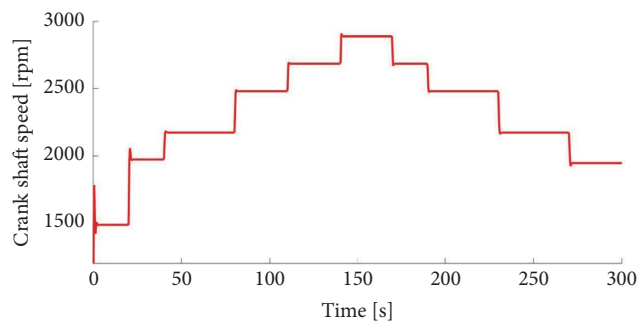

Figure 3: Crank shaft speed of the IC engine.

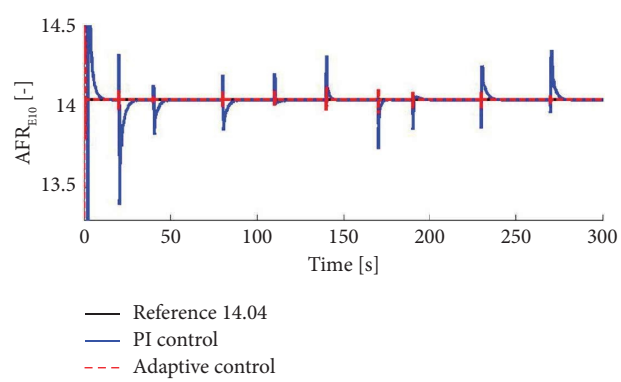

Figure 4: AFR control for the E10 blend.

Table 3: AFR_{E10} and $AFR_{overall}$ control errors.

	RMS	MSE
$AFR_{E_{10}}$ PI control	0.0196	0.0757
$AFR_{E_{10}}$ Adaptive control	0.008	0.0126
$AFR_{overall}$ PI control	0.0214	0.0983
$AFR_{overall}$ Adaptive control	0.0079	0.0133

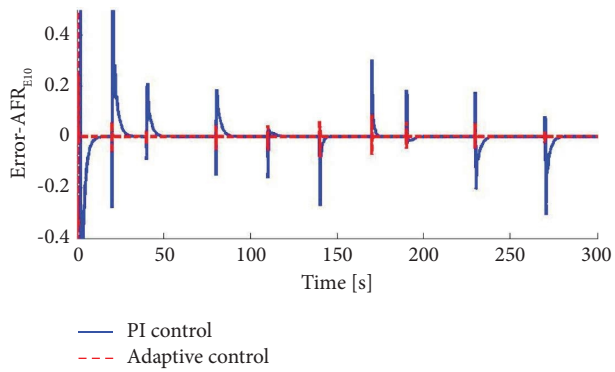

Figure 5: AFR control error for the E10 blend.

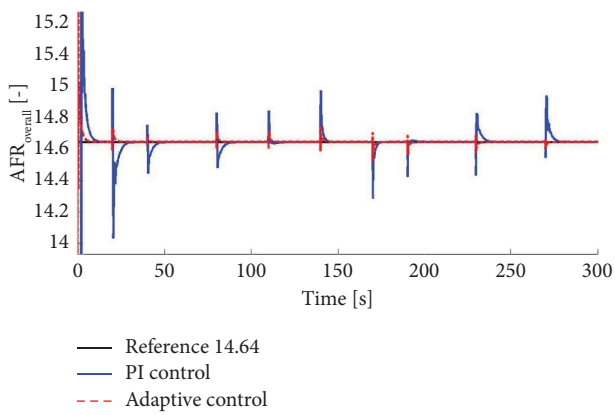

Figure 6: AFR control for the hydrogen-enriched E10 blend.

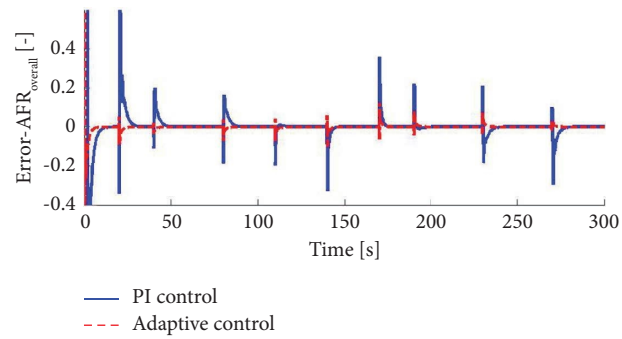

Figure 7: Overall AFR control error for the hydrogen-enriched E10 blend.

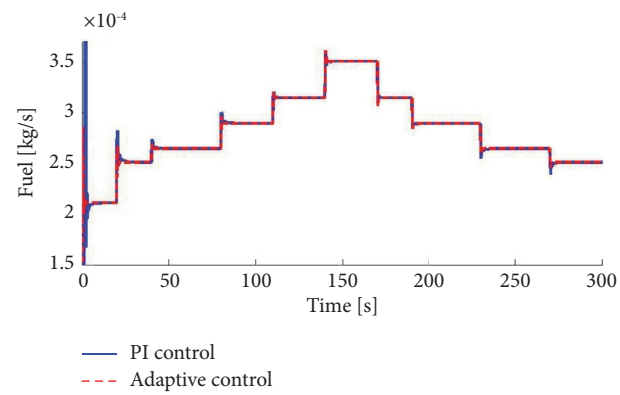

Figure 8: Fuel mass flow rate.

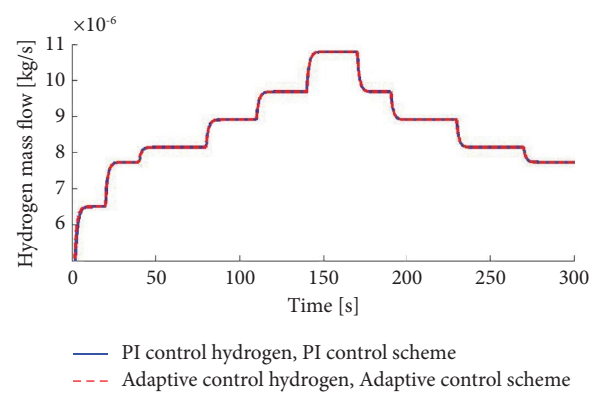

Figure 9: Hydrogen mass flow rate.

with a PI controller performance by using the mean squared error and the root mean square error. The results are shown in Table 3.

The adaptive controller evaluation for controlling the overall $AFR_{overall}$ is complemented in Figure 7. Figure 7 shows the AFR-o error analysis using a hydrogen-enriched E10 blend to feed the IC engine, and the error is the difference between the setpoint and the controlled signal of $AFR_{overall}$. As is shown in the figure, the $AFR_{overall}$ error tends to zero because the controlled signal reaches the setpoint. Note that the adaptive control action is faster than the PI control action since the adaptive control error converges to zero before the PI error.

The mass flow rate of the E10 blend supplied to the IC engine is shown in Figure 8. The figure shows that the overshoots reduced in magnitude using the adaptive controller compared with the overshoots generated by the PI controller. Thus, by using the proposed adaptive control, the engine performance is improved due to its rapid control action. On the other hand, the fuel consumption remains equal for both control strategies because they are bounded to use the same hydrogen amount.

Figure 9 shows the hydrogen mass flow rate production. In the red line is shown the hydrogen production using a PI control scheme. In the blue line is represented the hydrogen production using an adaptive control scheme. The hydrogen production depends on the air mass flow rate entering into the IC engine so that the adaptive controller does not affect the performance of the hydrogen production since the adaptive controller only affects the E10 blend fuel injection. The hydrogen mass flow rate varies from 4.059×10^{-6} to 1.088×10^{-5} according to the IC engine operating point.

Figure 10 shows the IC engine thermal efficiencies. According to the authors in [16],by using the hydrogen-enriched E10 blend, the thermal efficiency increases by 7.8% with respect to the use of pure gasoline. The IC engine efficiency was evaluated using the hydrogen-enriched E10 blend by applying a PI controller and adaptive controller. The results showed that applying the adaptive control law, the thermal efficiency's overshoots decreased in a considerable form

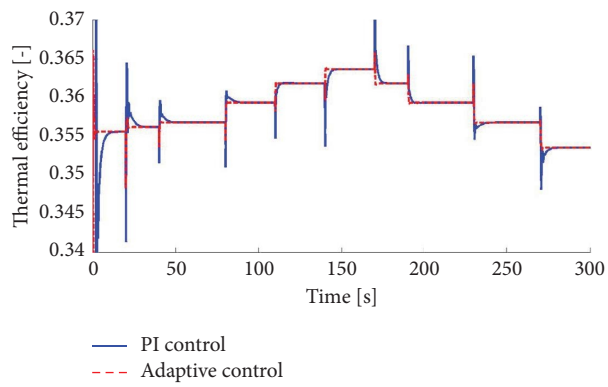

Figure 10: Thermal efficiency.

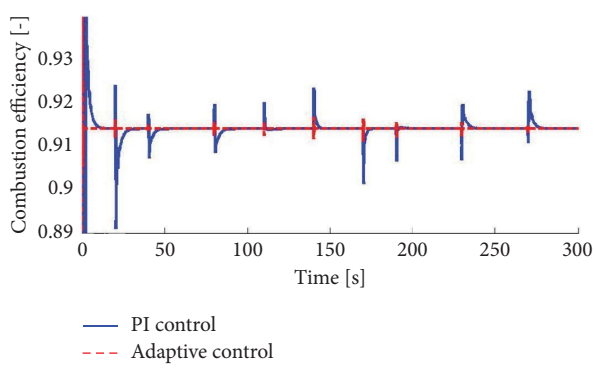

Figure 11: Combustion efficiency.

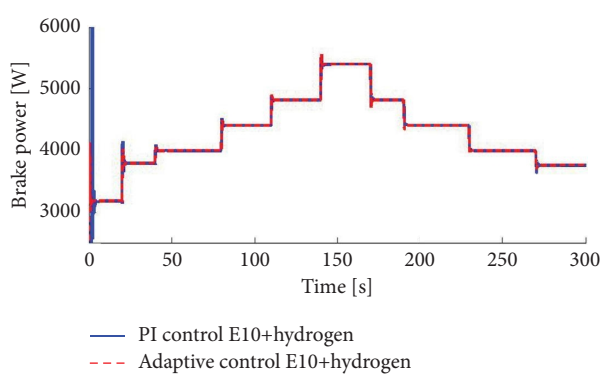

Figure 12: Brake power.

compared with the PI controller. The simulation was carried out in three different operating points of the IC engine (at 1500 rpm, at 2000 rpm, and 2900 rpm).

Figure 11 shows the IC engine combustion efficiency using a hydrogen-enriched E10 blend. According to the authors in [16], the combustion efficiency increases when it is used with the hydrogen-enriched E10 blend due to the ethanol burning velocity and hydrogen. Another reason is the high diffusibility of hydrogen. The figure shows that in the steady-state, both controllers had similar performances using the hydrogen-enriched E10 blend as a fuel. However, the adaptive controller had a better performance in the transient state since its control action is faster than the PI controller.

Figure 12 shows the brake power of the IC engine using the hydrogen-enriched E10 blend and applying a PI controller and the adaptive controller. In the steady state, the behavior of both signals was very similar. However, in the transient state, there were slight differences.

5. Conclusions

In conclusion, the adaptive controller presented a fast response to the operating point changes. The overshoot magnitudes in the AFR control were smaller than those obtained by the PI controller. The burning process in the internal combustion engine could be improved at any operating point due to the rapid control action of the adaptive controller. The AFR control improvement could reduce gasoline consumption and pollutant gas emission. Note that the control law could not have optimal behavior in an internal combustion engine implementation. It could happen due to structural and measurement uncertainties. In this case, the model should be reparametrized. For future works, to test the IC engine performance fueled with the hydrogen-enriched E10 blend, the adaptive controller will be experimentally implemented, as well as a timed ignition control.

Data Availability

Internal combustion engine simulation data used to support the findings of this study are available from the corresponding author upon request.

Conflicts of Interest

The authors declare that they have no conflicts of interest.

Acknowledgments

The authors would like to thank the ITS de las Choapas for the financial support for the publication of this manuscript. Likewise, the authors thank PRODEP, Tecnológico Nacional de México, and CENIDET for their help in developing this work. José Francisco Gómez Aguilar acknowledges the support provided by Conacyt: cátedras CONACyT para jóvenes investigadores 2014.

References

[1] D. A. Carbot-Rojas, R. F. Escobar-Jiménez, J. F. Gómez-Aguilar, J. García-Morales, and A. C. Téllez-Anguiano, "Modelling and control of the spark timing of an internal combustion engine based on an ann," *Combustion Theory and Modelling*, vol. 24, no. 3, pp. 510–529, 2020.

[2] D. A. Carbot-Rojas, R. F. Escobar-Jiménez, J. F. Gómez-Aguilar, and A. C. Téllez-Anguiano, "A survey on modeling, biofuels, control and supervision systems applied in internal combustion engines," *Renewable and Sustainable Energy Reviews*, vol. 73, pp. 1070–1085, 2017.

[3] R. Escobar-Jiménez, M. Cervantes-Bobadilla, J. García-Morales, J. Gómez Aguilar, J. Hernández Pérez, and A. Alvarez-Gallegos, "Short communication: the effects of not controlling the hydrogen supplied to an internal combustion engine," *International Journal of Hydrogen Energy*, vol. 45, no. 29, 2020.

[4] P. Kaidantzis, P. Rasmussen, M. Jensen, T. Vesterholm, and E. Hendricks, "Advanced nonlinear observer control of SI engines," *Journal of Engines*, vol. 102, 1993.

[5] J. D. Powell, N. P. Fekete, and C. F. Chang, "Observer-based air fuel ratio control," *IEEE Control Systems*, vol. 18, no. 5, pp. 72–83, 1998.

[6] M. Zohari, M. Ahmadi, and H. Mojallali, "Dynamic sliding mode control of air-to-fuel ratio in internal combustion engines using the hybrid extended kalman filter," *Advanced Materials Research*, vol. 433, pp. 2092–2098, 012.

[7] W. Xue, W. Bai, S. Yang, K. Song, Y. Huang, and H. Xie, "ADRC with adaptive extended state observer and its application to air-fuel ratio control in gasoline engines," *IEEE Transactions on Industrial Electronics*, vol. 62, no. 9, pp. 5847–5857, 2015.

[8] U. Lenz and D. Schroeder, "Transient air-fuel ratio control using artificial intelligence," *Training*, vol. 2014, 1997.

[9] J. Lauber, T. M. Guerra, and M. Dambrine, "Air-fuel ratio control in a gasoline engine," *International Journal of Systems Science*, vol. 42, no. 2, pp. 277–286, 2011.

[10] P. K. Wong, H. C. Wong, C. M. Vong, Z. Xie, and S. Huang, "Model predictive engine air-ratio control using online sequential extreme learning machine," *Neural Computing & Applications*, vol. 27, no. 1, pp. 79–92, 2016.

[11] C. Khajorntraidet and K. Ito, "Simple adaptive air-fuel ratio control of a port injection SI engine with a cylinder pressure sensor," *Control Theory and Technology*, vol. 13, no. 2, pp. 141–150, 2015.

[12] N. E. Kahveci, S. T. Impram, and A. U. Genc, "Air-fuel ratio regulation using a discrete-time internal model controller," in *Intelligent Transportation Systems (ITSC), 2014 IEEE 17th International Conference on IEEE*, pp. 2459–2464, IEEE, Qingdao, China, 2014.

[13] Y. Yildiz, A. Annaswamy, D. Yanakiev, and I. Kolmanovsky, "Adaptive air fuel ratio control for internal combustion engines," in *American Control Conference*, pp. 2058–2063, IEEE, Seattle, WA, USA, 2008.

[14] R. C. Turin and H. P. Geering, "Model-reference adaptive A/F-ratio control in an SI engine based on kalman-filtering techniques,"vol. 6, pp. 4082–4090, in *Proceedings of the American Control Conference*, vol. 6, pp. 4082–4090, IEEE, Seattle, WA, USA, 1995.

[15] J. G. Morales, M. C. Bobadilla, R. F. Escobar-Jiménez, J. F. Gómez-Aguilar, C. D. García-Beltrán, and V. H. Olivares-Peregrino, "Control scheme formulation for the production of hydrogen on demand to feed an internal combustion engine," *Sustainability*, vol. 9, no. 1, p. 7, 2016.

[16] J. García-Morales, M. Cervantes-Bobadilla, R. F. Escobar-Jímenez, J. F. Gómez-Aguilar, and V. H. Olivares-Peregrino, "Experimental implementation of a control scheme to feed a hydrogen-enriched E10 blend to an internal combustion engine," *International Journal of Hydrogen Energy*, vol. 42, no. 39, pp. 25026–25036, 2017.

[17] A. A. Amin and K. Mahmood-ul Hasan, "Unified fault-tolerant control for air-fuel ratio control of internal combustion engines with advanced analytical and hardware redundancies," *Journal of Electrical Engineering & Technology*, vol. 17, no. 3, pp. 1947–1959, 2021.

[18] A. A. Amin and K. Mahmood-ul Hasan, "Robust passive fault tolerant control for air fuel ratio control of internal combustion gasoline engine for sensor and actuator faults," *IETE Journal of Research*, pp. 1–16, 2021.

[19] S. Coşkun and E. Köse, "Lean-burn air-fuel ratio control using genetic algorithm-based pi controller," *International Journal of Advances in Engineering & Technology*, vol. 10, no. 3, pp. 126–134, 2021.

[20] Z. Salehi, S. Azadi, and A. Mousavinia, "Sliding mode air-to-fuel ratio control of spark ignition engines in comprehensive powertrain system," in *2021 7th International Conference on Control, Instrumentation and Automation (ICCIA)*, pp. 1–5, IEEE, Tabriz, Iran, 2021.

[21] D. Song and Y. Li, "Predictive control of transient air-fuel ratio for gasoline engine based on wavelet network inversion," in *IOP Conference Series: Earth and Environmental Science*, vol. 508, 2020, Article ID 012052.

[22] C. F. Aquino, "Transient A/F control characteristics of the 5 liter central fuel injection engine," *SAE Technical Paper*, vol. 90, 1981.

[23] L. Guzzella and C. Onder, *Introduction to Modeling and Control of Internal Combustion Engine System*, Springer, Berlin, Germany, 2010.

[24] W. Zhihu and P. Run, "Torque based spark ignition engine and powertrain modeling," in *Proceedings of the 7th World Congress on Intelligent Control and Automation*, pp. 4767–4772, Chongqing, China, 2008.

[25] B. Mashadi and D. Crolla, *Vehicle Powertrain Systems*, John Wiley and Sons, San Francisco, CA, USA, 2012.

[26] E. Hendricks and S. Sorenson, "Mean value modeling of spark ignition engines," *SAE Technical Paper*, Warrendale, PA, USA, SAE, 1990.

[27] I. Schifter, L. Diaz, R. Rodriguez, J. Gómez, and U. Gonzalez, "Combustion and emissions behavior for ethanol–gasoline blends in a single cylinder engine," *Fuel*, vol. 90, no. 12, pp. 3586–3592, 2011.

[28] J. M. Mantilla, *Modelado de la combustión de mezclas gasolina-etanol en motores de combustión interna*, Ph.D. thesis, Universidad Nacional de Colombia, Bogotá, Colombia, 2010.

[29] G. P. Blair, *Design and Simulation of Two-Stroke Engines*, Society of Automotive Engineers Warrendale, Pittsburgh, PA, USA, 1996.

[30] L. Eugene, W. Kevin, and D. Howe, *Robust and Adaptive Control with Aerospace Applications*, Springer, London, UK, 2012.

[31] R. Yan, H. Li, Z. Y. Dong, and H. Tang, "Nonlinear control approaches for si engine model with uncertainties," in *Proceedings of the 48h IEEE Conference on Decision and Control (CDC) Held Jointly with 2009 28th Chinese Control Conference*, pp. 5440–5445, IEEE, Shanghai, China, 2009.